

CCD Photometry, Light Curve Deconvolution, Period Analysis, Kinematics, and Evolutionary Status of the HADS Variable V460 Andromedae

Kevin B. Alton

UnderOak and Desert Bloom Observatories, 70 Summit Avenue, Cedar Knolls, NJ 07927; kbalton@optonline.net

Kazimierz Stepień

Warsaw University Observatory, Al. Ujazdowskie 4, 00-478 Warszawa, Poland

Received March 3, 2019; revised April 8, 2019; accepted April 8, 2019

Abstract Multi-color (BVI_c) CCD-derived photometric data were acquired from V460 And, an intrinsic variable classically defined as a High Amplitude delta Scuti (HADS) type system. Deconvolution of precise time-series light curve data was accomplished using discrete Fourier transformation and revealed a fundamental mode (f_0) of oscillation at ~ 13.336 d⁻¹ along with five other partial harmonics ($2f_0$ – $6f_0$). No other statistically significant frequencies were resolved following successive pre-whitening of each residual signal. An assessment of potential period changes over time was performed using six new times-of-maximum light produced from the present study along with other values reported in the literature. These along with sparsely-sampled data collected during the ROTSE-I (1999), Catalina Sky (2005–2013), and SuperWASP (2004–2008) surveys indicate that no substantive change in the primary pulsation period or amplitude (V-mag) has likely occurred over the past 20 years. Recent photometric data from space telescopes have in some cases contradicted traditional classification schemes and clouded the differences between HADS- and SX Phe-like variables. Herein using accurate cosmic distances and proper motions from Gaia DR2, we attempted to exploit potential kinematic differences between established populations of HADS and SX Phe variable stars as an alternate approach for classification. Finally, an investigation with PARSEC models for generating stellar tracks and isochrones provided valuable insight into the evolutionary status and physical character of V460 And.

1. Introduction

The most common A- and F-type stars which exhibit variability are the multi-periodic pulsators known as delta Scuti-like (hereafter δ Sct) stars. As a class these intrinsic variables occupy a narrow area at the intersection of the classical instability strip, pre-main-sequence, and main-sequence (MS) on the Hertzsprung-Russell diagram. Therein they represent a transition from the high-amplitude radial pulsators, such as Cepheid variables, and non-radial multi-periodic pulsators (Breger 2000). Main-sequence δ Sct stars typically range from spectral type F2 to A2 (Rodríguez and Breger 2001), which corresponds to effective temperatures varying between 6300 and 8600 K (Uytterhoeven *et al.* 2011). Hotter δ Sct stars generally have shorter pulsation periods (i.e. higher pulsation mode frequencies) than cooler δ Sct stars.

Similar to Cepheid and RR Lyrae stars (Baker and Kippenhahn 1962, 1965; Zhevakin 1963), pulsations in δ Sct stars are excited by the κ -mechanism operating in the He II partial ionization zone ($T \sim 50000$ K) which produce low-order pressure (p) modes akin to acoustic waves (Cox 1963; Chevalier 1971). These can produce radial pulsations which evoke symmetrical changes in stellar size and/or non-radial pulsations that give rise to asymmetric changes in shape but not volume. Although shorter periods (< 30 min) have been observed (Holdsworth *et al.* 2014) in some A-type stars, the fundamental radial pulsations of Galactic δ Sct variables with near solar metallicity typically range from 0.05 to 0.25 d. Masses vary from $\sim 1.2 M_{\odot}$ to $\sim 2.5 M_{\odot}$ so they are more luminous and larger than our Sun. The luminosity classes for δ Sct variables generally range from III (normal giants) to V (MS stars). δ Sct variables with

moderate (40 km s^{-1}) to rapid (250 km s^{-1}) rotational velocities ($v \sin i$) generally have small light amplitudes ($\Delta V \sim 0.01$ – 0.03 mag) composed of a multitude of pulsation frequencies, most of them nonradial. Stars with slow rotational velocities ($< 30 \text{ km s}^{-1}$) tend to be radial pulsators and have light amplitudes (V-mag) in excess of 0.20–0.30 mag. The latter characteristics define a δ Sct subgroup called High-Amplitude delta Scuti stars (HADS).

HADS represent a very small fraction ($< 1\%$) of all δ Sct variables (Lee *et al.* 2008). They commonly oscillate via low-order single or double radial pulsation modes (Poretti 2003a, 2003b; Niu *et al.* 2013, 2017). A high percentage ($\sim 40\%$) are double pulsators showing simultaneous pulsations in the fundamental and the first overtone mode with amplitudes generally higher in the fundamental mode (McNamara 2000). It should be noted, however, that non-radial pulsations have also been detected with the HADS variable V974 Oph (Poretti 2003a, 2003b). HADS variables have historically been divided according to metallicity relative to our Sun ($[Fe/H] = 0$ dex). The metal-poor ($[Fe/H] \ll 0$) group is called SX Phe stars based on the eponymous prototype SX Phoenicis. Ostensibly they have shorter periods ($0.02 < P < 0.125$ d) and lower masses (~ 1.0 – $1.3 M_{\odot}$) than their sibling HADS variables possessing near solar metal abundance. SX Phe stars frequently dwell in globular clusters (GC), ancient collections of Population I stars. Therein, the majority of SX Phe variables are classified as blue straggler stars, paradoxically appearing much younger than their GC cohorts. Despite previous claims to the contrary, Balona and Nemeč (2012) make a strong case that it is not possible to differentiate between δ Sct and field SX Phe variables based on pulsation amplitude, the number of pulsation modes, period,

or even metallicity. Much more sensitive space telescopes like Kepler (Gilliland *et al.* 2010), CoRoT (Baglin 2003), and MOST (Walker *et al.* 2003) have found many examples that violate these basic tenants. They further argue that the evolutionary status of each star is the only way to distinguish between these two classes. One way to get a handle on the age of a star is to exploit potential differences in kinematics. Population II stars often reside away from the Galactic plane in globular clusters, the halo, and thick disc. Arguably, pulsating field stars that reside in these regions of the Milky Way will have high proper motions (μ_α, μ_δ) but more importantly greater tangential velocities ($V_{T_\alpha}, V_{T_\delta}$) than younger MS (Population I) δ Sct variables occupying the thin disk. As will be discussed herein, the availability of very precise proper motion (PM) and parallax values from Gaia DR2 has for the moment muddled the water with regard to differentiation between HADS and SX Phe variables.

The putative variability of V460 And (GSC 02840-01177) was first identified based on an entry (No. 227) in the *Catalogue of the Stars of Suspected Variability* (Kukarkin *et al.* 1951). Its variable nature was further reported (Kinman *et al.* 1982) based on photographic plates taken between 1962 and 1968 but no variable type assignment could be made from the star identified as RRV-26. Following an evaluation of unfiltered photometric data from the ROTSE-I Survey (Akerloft *et al.* 2000), Khruslov (2005) reported that V460 And (NSVS 4000553) was a HADS star with a period of 0.0749808 d. Photometric (V-mag) data from V460 And (CSS_J023414.3+421427) were also acquired during the Catalina Sky Survey (Drake *et al.* 2009); an assessment herein of the CSS data further confirmed the fundamental period reported by Khruslov (2005). This report marks the first multi-color photometric study on V460 And which also addresses a longstanding, but unproven classification as a HADS variable.

2. Observations and data reduction

2.1. Photometry

Time-series images were acquired at Desert Bloom Observatory (DBO, USA—110.257 W, 31.941 N) with an SBIG STT-1603ME CCD camera mounted at the Cassegrain focus of a 0.4-m Schmidt-Cassegrain telescope. This focal-reduced (f/6.8) instrument produces an image scale of 1.36 arcsec/pixel (bin=2×2) and a field-of-view (FOV) of 11.5'×17.2'. Image acquisition (75-s) was performed using THE SKYX Professional Edition 10.5.0 (Software Bisque 2019). The CCD-camera is equipped with B, V, and I_c filters manufactured to match the Johnson-Cousins Bessell specification. Dark subtraction, flat correction, and registration of all images collected at DBO were performed with AIP4WIN v2.4.0 (Berry and Burnell 2005). Instrumental readings were reduced to catalog-based magnitudes using the APASS star fields (Henden *et al.* 2009, 2010, 2011; Smith *et al.* 2011) built into MPO CANOPUS v10.7.1.3 (Minor Planet Observer 2011). Light curves for V460 And were generated using an ensemble of five non-varying comparison stars. The identity, J2000 coordinates, and APASS color indices (B–V) for these stars are provided in Table 1; a corresponding FOV image is rendered in Figure 1. Only data from images

Table 1. Astrometric coordinates (J2000), V-mag, and color indices (B–V) for V460 And and five comparison stars (1–5) used during this photometric study.

FOV ID	Star Identification	R.A. h m s	Dec. ° ' "	APASS ^a V-mag	APASS ^a (B–V)
T	V460 And	02 34 14.255	+42 14 27.604	13.168	0.238
1	GSC 02840-01355	02 34 05.770	+42 14 05.009	12.334	0.549
2	GSC 02840-01209	02 33 55.975	+42 12 15.444	12.613	0.642
3	GSC 02840-01660	02 33 55.617	+42 08 14.655	12.225	0.578
4	GSC 02840-01826	02 33 04.906	+42 09 43.343	11.767	0.309
5	GSC 02840-00853	02 33 58.663	+42 11 00.420	13.354	0.685

^aV-mag and (B–V) for comparison stars derived from APASS database described by Henden *et al.* (2009, 2010, 2011) and Smith *et al.* (2010), as well as on the AAVSO web site (<https://www.aavso.org/apass>).

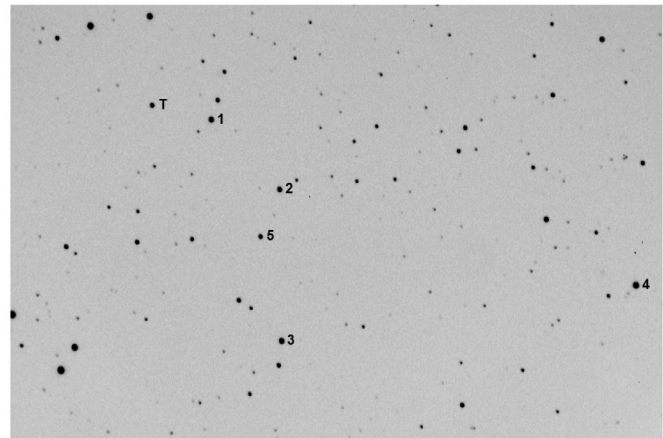


Figure 1. V460 And (T) along with the five comparison stars (1–5) used to reduce time-series images to APASS-catalog based magnitudes.

taken above 30° altitude (airmass < 2.0) were included; considering the proximity of all program stars, differential atmospheric extinction was ignored. During each imaging session comparison stars typically stayed within ±0.006 mag for V and I_c filters and ±0.009 mag for the B passband.

3. Results and discussion

3.1. Photometry and ephemerides

Photometric values in B (n=155), V (n=153), and I_c (n=150) passbands were separately processed to produce light curves that spanned 4 days between Dec 19 and Dec 23, 2018 (Figure 2). There was no obvious color dependency on the timings such as those reported for other δ Sct variables (Elst 1978); therefore, all BVI_c data were averaged (Table 2) at each time-of-maximum. Period determinations were initially performed using PERANSO v2.5 (Paunzen and Vanmunster 2016) by applying periodic orthogonals (Schwarzenberg-Czerny 1996) to fit observations and analysis of variance (ANOVA) to assess fit quality. In this case a similar period solution for each passband (0.07498 ± 0.00001 d) was obtained. However, folding together (time span = 7,102 d) the sparsely sampled ROTSE-I and Catalina Sky survey data with those (V-mag) acquired at DBO yielded a period at 0.0749808 ± 0.0000010 d (Figure 3). Additionally, the SuperWASP survey (Butters *et al.* 2010) provided a rich source of photometric data taken (30-s exposures) at modest cadence

Table 2. Differences between the times-of-maximum light (HJD) predicted from the updated linear ephemeris (Equation 2) and those observed for V460 And between 2007 and 2018. Cycle No. is determined from the number of pulsations that have occurred since the start time (HJD₀) defined by the reference ephemeris.

HJD 2400000+	Cycle No.	FPPTD ^a	Ref. ^b	HJD 2400000+	Cycle No.	FPPTD ^a	Ref. ^b
54135.3080	35745	0.0066	1	55894.2830	59204	0.0065	5
54135.3831	35746	0.0067	1	55894.3580	59205	0.0071	5
54355.5266	38682	0.0067	1	55894.4330	59206	0.0079	5
54355.6013	38683	0.0064	1	55894.5813	59208	0.0079	4
54391.4424	39161	0.0067	1	55894.6564	59209	0.0079	4
54391.5180	39162	0.0073	1	55894.7316	59210	0.0062	4
54391.5923	39163	0.0066	1	55894.8064	59211	0.0064	4
55192.3112	49842	0.0060	2	55894.8812	59212	0.0066	4
55192.3863	49843	0.0061	2	55894.9565	59213	0.0064	4
55452.3457	53310	0.0072	3	55897.2054	59243	0.0062	4
55452.4202	53311	0.0067	3	55897.2808	59244	0.0065	4
55452.4947	53312	0.0062	3	55897.3556	59245	0.0060	4
55452.5701	53313	0.0066	3	56176.5845	62969	0.0064	6
55590.3099	55150	0.0068	4	56176.6597	62970	0.0063	6
55590.3844	55151	0.0063	4	56254.2645	64005	0.0068	6
55590.4591	55152	0.0060	4	56506.5001	67369	0.0070	7
55850.3430	58618	0.0066	5	56566.3358	68167	0.0067	7
55850.5690	58621	0.0076	5	56566.4090	68168	0.0070	7
55856.2666	58697	0.0067	4	56635.3161	69087	0.0081	8
55856.3408	58698	0.0059	4	56742.3147	70514	0.0063	9
55889.6329	59142	0.0066	4	56912.4453	72783	0.0061	9
55889.7076	59143	0.0063	4	56912.5204	72784	0.0071	9
55889.7826	59144	0.0063	4	56962.3075	73448	0.0064	9
55889.8579	59145	0.0066	4	56962.3832	73449	0.0065	9
55889.9325	59146	0.0062	4	57000.4732	73957	0.0064	9
55890.0072	59147	0.0060	4	57006.3208	74035	0.0071	9
55893.6067	59195	0.0064	4	58471.5951	93577	0.0069	10
55893.6820	59196	0.0067	4	58471.6708	93578	0.0060	10
55893.7568	59197	0.0065	4	58473.6204	93604	0.0061	10
55893.8316	59198	0.0063	4	58473.6951	93605	0.0069	10
55893.9067	59199	0.0065	4	58475.6441	93631	0.0070	10
55893.9823	59200	0.0071	4	58475.7196	93632	0.0067	10

^aFPPTD = Time difference between observed fundamental pulsation time-of-maximum and that calculated using the reference ephemeris (Equation 2).
^b1. Wils et al. 2009; 2. Wils et al. 2010; 3. Wils et al. 2011; 4. Wils et al. 2012; 5. Hübscher and Lehmann 2012; 6. Wils et al. 2013; 7. Wils et al. 2014; 8. Hübscher 2014; 9. Wils et al. 2015; 10. This study.

that repeats every 9–12 min. These data acquired between 2004 and 2008 were period folded with V-mag data collected at DBO and crisply reached superimposition when P=0.0749807 d (Figure 4). Times-of-maximum light acquired at DBO were estimated using the polynomial extremum fit utility featured in PERANSO (Paunzen and Vanmunster 2016). New maxima from DBO (6) along with published values starting in 2007 (Table 2) were used to analyze fundamental pulse period timings (FPPT). The reference epoch (International Variable Star Index) adopted for initially calculating FPPT differences (FPPTD) was defined by the following linear ephemeris (Equation 1):

$$\text{Max (HJD)}=2451455.114+0.0749808E. \quad (1)$$

Secular changes in pulsation period can potentially be uncovered by plotting the difference between the observed FPPT values and those predicted by the reference epoch against cycle number (Figure 5). Thus far, all of the calculated FPPTD values (Table 4) basically describe a straight line relationship

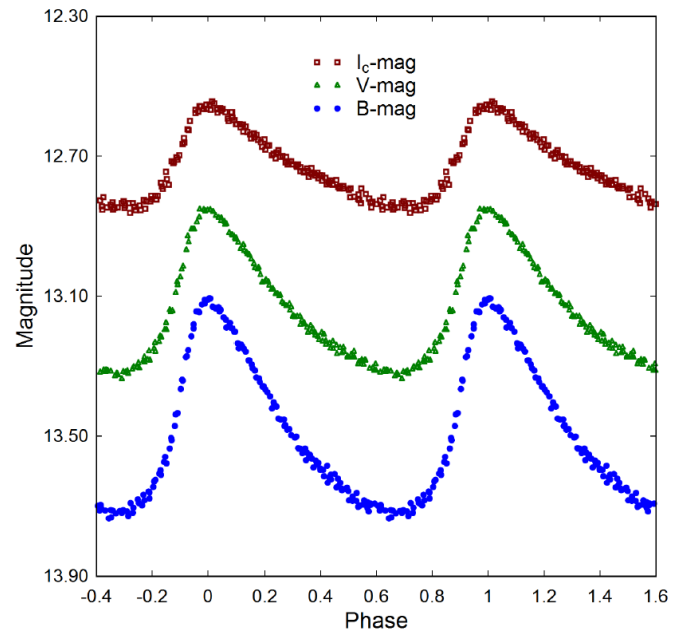


Figure 2. Period-folded (0.0749808 d) light curves for V460 And produced from photometric data obtained between Dec 19 and Dec 23, 2018 at DBO. Light curves shown at the top (I_c), middle (V) and bottom (B) represent catalog-based (APASS) magnitudes determined using MPO CANOPUS.

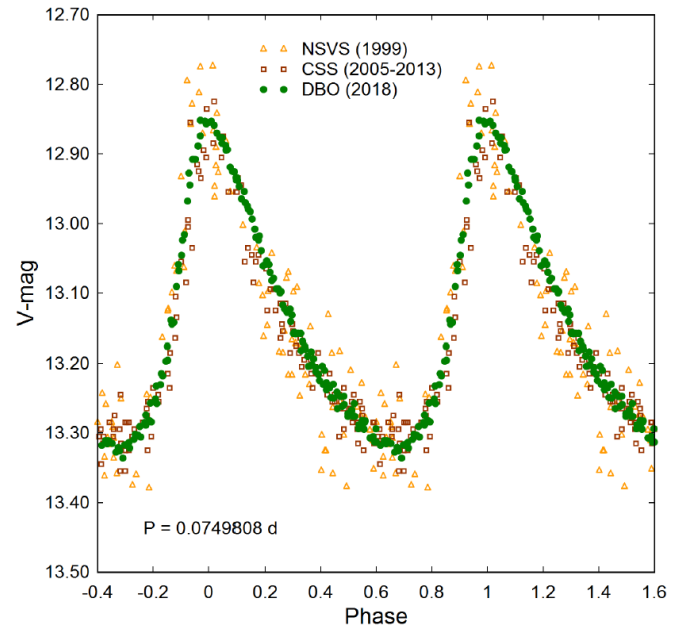


Figure 3. Period-folded (0.0749808 d) light curves for V460 And produced from precise photometric V-mag data obtained at DBO (2018) along with sparsely sampled data from the ROTSE-I (1999) and Catalina Sky (2005-2013) Surveys. Magnitudes were offset to conform with the APASS-derived values from DBO.

(albeit noisy) and suggest that little or no long-term change to the period has occurred since 1999. The updated ephemeris (Equation 2) based on maximum light timing data available through Dec 2018 is as follows:

$$\text{Max (HJD)}=2458475.7195(3)+0.07498076(5)E. \quad (2)$$

These results along with nearly superimposable period-folded light curves from DBO, ROTSE-I, CSS (Figure 3), and

Table 3. Fundamental frequency ($f_0 = \text{d}^{-1}$) and corresponding partial harmonics detected following DFT analysis of time-series photometric data (BVI) from V460 And.

	Freq. (d^{-1})	Freq. Err	Amp. (mag)	Amp. Err	Phase	Phase Err
$f_0\text{-B}$	13.3367	0.0002	0.2682	0.0011	0.2609	0.1497
$f_0\text{-V}$	13.3363	0.0003	0.2045	0.0010	0.9024	0.1627
$f_0\text{-I}_c$	13.3361	0.0004	0.1255	0.0012	0.7262	0.1223
$2f_0\text{-B}$	26.6786	0.0007	0.0909	0.0011	0.6918	0.1566
$2f_0\text{-V}$	26.6786	0.0008	0.0721	0.0010	0.9546	0.1672
$2f_0\text{-I}_c$	26.6793	0.0011	0.0463	0.0012	0.7583	0.1286
$3f_0\text{-B}$	40.0132	0.0017	0.0368	0.0011	0.1365	0.1517
$3f_0\text{-V}$	40.0093	0.0022	0.0269	0.0009	0.1198	0.1555
$3f_0\text{-I}_c$	40.0069	0.0026	0.0184	0.0011	0.8465	0.1209
$4f_0\text{-B}$	53.3430	0.0034	0.0198	0.0010	0.8096	0.1588
$4f_0\text{-V}$	53.8247	0.0043	0.0131	0.0009	0.4156	0.1482
$4f_0\text{-I}_c$	52.8671	0.0056	0.0091	0.0011	0.4305	0.1189
$5f_0\text{-B}$	66.6847	0.0058	0.0105	0.0011	0.7239	0.1478
$5f_0\text{-V}$	66.6726	0.0083	0.0072	0.0009	0.6484	0.1630
$6f_0\text{-B}$	80.0145	0.0083	0.0073	0.0011	0.4521	0.1540
$6f_0\text{-V}$	80.0359	0.0170	0.0042	0.0009	0.6981	0.1633

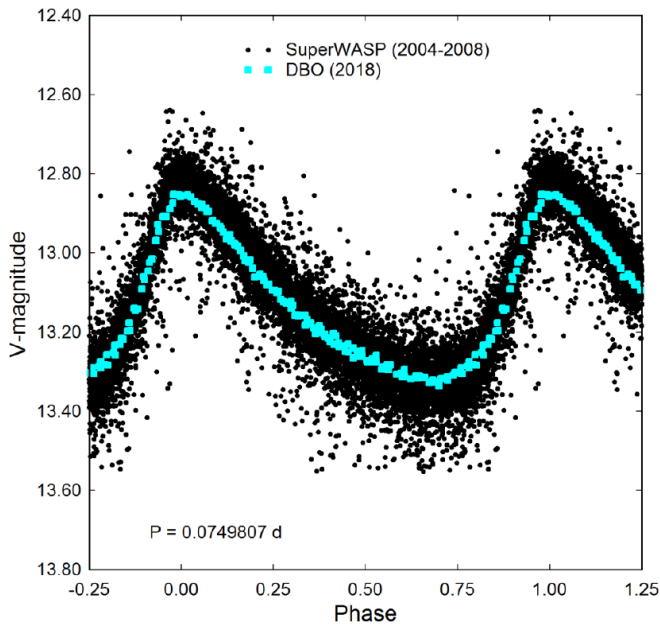


Figure 4. Period-folded (0.0749807 d) light curves for V460 And produced from precise photometric V-mag data obtained at DBO (2018) along with broad-band (400–700 nm) data from the SuperWASP Survey (2004–2008). Magnitudes were offset to conform with the APASS-derived values from DBO.

SuperWASP (Figure 4) make a strong case that the fundamental pulsation period has not substantively changed since 1999 nor has the V-mag amplitude changed significantly over the same period of time.

3.2. Light curve behavior

Morphologically, light curves from HADS variables are asymmetrical with a faster rise time from minimum to maximum light than the decline back to minimum brightness. V460 And appears to be a textbook example in this regard (Figure 2). The largest difference between maximum and minimum light is observed in the blue passband ($\Delta B\text{-mag} = 0.61$), followed by V ($\Delta V\text{-mag} = 0.47$), and finally the smallest difference in infrared

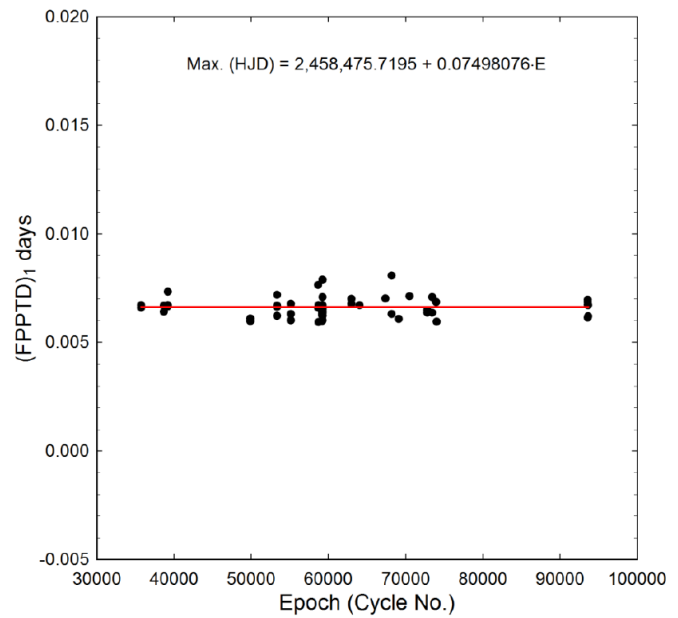


Figure 5. Straight line fit (FPPTD vs. period cycle number) suggesting that little or no change to the fundamental pulsation period of V460 And had occurred between 1999 and 2018.

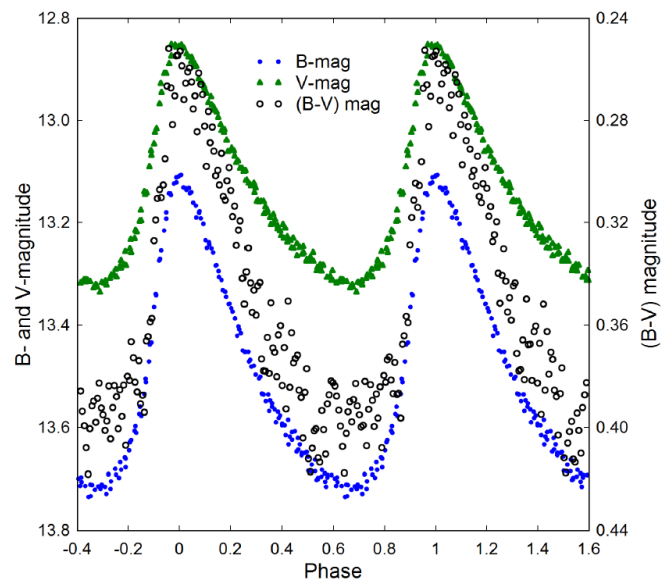


Figure 6. V460 And light curves illustrating significant increase in reddening ($0.261 < (B-V) < 0.393$) as maximum light slowly descends to minimum light. This effect is most closely associated with a decrease in the effective surface temperature during minimum light.

($\Delta I_c\text{-mag} = 0.29$). This behavior is typical for pulsating F- to A-type stars. It follows when the B- and V-mag light curves are divided into equal phase intervals and then subtracted from one another, the emerging light curve ($B-V$) exhibits significant reddening during minimum light (Figure 6). In this case color excess ($B-V$) ranges between 0.261 and 0.393 mag. Estimates for interstellar extinction (A_V) vary widely depending on the model selected (Amôres and Lépine 2005, 2007; Burstein and Heiles 1978, 1982; Schlegel *et al.* 1998; Schlafly and Finkbeiner 2011; Drimmel *et al.* 2003). Access to these data is greatly facilitated via the GALextin website at <http://www.galexin.org/v1p0/>. The median reddening value

($E(B-V)=0.0803 \pm 0.0006$ mag), coincidentally from Schlegel *et al.* (1998), corresponds to an intrinsic color index $(B-V)_0$ for V460And that varies between 0.181 ± 0.006 at maximum light and 0.313 ± 0.010 mag at minimum brightness. Based on the polynomial transformation equations derived by Flower (1996) with the misprints corrected by Torres (2010), the mean effective temperature (T_{eff}) was estimated to be 7385 ± 520 K, with a minimum T_{eff} of $\sim 7150 \pm 229$ K and a maximum T_{eff} of $\sim 7880 \pm 263$ K. These results based strictly on $(B-V)$ photometry at DBO are in good agreement with the findings for V460And ($T_{\text{eff}}=7507_{-427}^{+339}$ K) included in the Gaia DR2 release of stellar parameters (Andrae *et al.* 2018). Furthermore, J- and K-band data from 2MASS (Skrutskie *et al.* 2006) when transformed according to Casagrande *et al.* (2010) predict a T_{eff} range between 7550 and 7100 K, depending on metallicity ($-2.0 < [\text{Fe}/\text{H}] \leq 0$). Although no verifiable classification spectra were found in the literature, the spectral type of this variable would likely range between A9 and F1.

3.3. Light curve analysis by Discrete Fourier Transformation

Light curve deconvolution was performed with PERIOD04 (Lenz and Breger 2005) wherein discrete Fourier transformation (DFT) was used to extract the fundamental pulsating frequency (spectral window = 100 d^{-1}). Pre-whitening steps which successively remove the previous most intense signals were employed to tease out other potential oscillations from the residuals. Only those frequencies with a $S/N \geq 4$ in each passband are presented in Table 3. In all cases, uncertainties in frequency, amplitude, and phase were estimated by the Monte Carlo simulation ($n=400$) routine built into PERIOD04.

The results strongly indicate that V460And is a monophasic radial pulsator; changes in stellar size during each pulsation cycle are therefore symmetrical. The spectral window and amplitude spectra derived from the B- and V-passband data are illustrated in Figure 7; others are not included since they are essentially redundant with respect to detected frequencies. As would be expected, the fundamental pulsation period ($f_0 \approx 13.336 \text{ d}^{-1} \approx 154.4 \mu\text{Hz}$) has the greatest amplitude. Successive pre-whitening steps uncovered partial harmonics out as far as $6f_0$; however, they were not statistically significant ($S/N < 4$) beyond $4f_0$ in the I_c -passband. The amplitude decay appears to be exponential as a function of harmonic order (Figure 8), a behavior that has been observed with other HADS variables such as VX Hya (Templeton *et al.* 2009) and RR Gem (Jurcsik *et al.* 2005). Although no other independent pulsation modes were detected during this short campaign, it is acknowledged that a longer baseline in time from multiple sites would be required to validate this claim (Breger 2000). Representative light curve fits to B-, V-, and I_c -mag time-series data (Dec 21, 2018) following DFT analysis are illustrated in Figure 8.

3.4. Global parameters

Pulsating stars have long served as standard candles for estimating cosmic distances to individual stars, clusters, and galaxies. One of the most important historical events in astronomy occurred when Henrietta Leavitt discovered a period-luminosity (P-L) relationship between 25 Cepheid variables

in the Small Magellanic Cloud (Leavitt and Pickering 1912). Since then this P-L relationship has been refined owing to differences between metal-rich (Population I) and metal-poor (Population II) Cepheids (Baade 1956). Like the Cepheids, other variable stars that pulsate via the κ -mechanism were found to obey distinct P-L relationships. Robust P-L relationships in the near infrared (Longmore *et al.* 1986) and mid-infrared (Neeley *et al.* 2015) for the ubiquitous RR~Lyrae-type variables have been established to estimate distances to globular clusters. The earliest descriptions of a P-L relationship for δ Sct variables were published by Frolov (1969) and Dworak and Zieba (1975). A more modern refinement of the P-L relationship for δ Sct variables was reported by McNamara (2011) albeit with Hipparcos parallaxes and not the more accurate values determined by the Gaia Mission (Lindgren *et al.* 2016; Gaia *et al.* 2016, 2018). Nonetheless this empirically-derived expression (Equation 3):

$$M_V = (-2.89 \pm 0.13) \log(P) - (1.31 \pm 0.10), \quad (3)$$

appears to correspond reasonably well to the main ridge of Gaia DR2-derived P-L data for δ Sct variables determined by Ziaali *et al.* (2018).

Absolute V_{mag} (M_V) was estimated (1.941 ± 0.177) after substituting the fundamental pulsation period P (0.07498076 d) into Equation 3. Using known values for m ($V_{\text{avg}} = 13.142 \pm 0.151$), $A_V = 0.2489 \pm 0.0019$, and M_V , the reddening corrected distance modulus (Equation 4):

$$d(\text{pc}) = 10^{(m - M_V - A_V + 5)/5}, \quad (4)$$

produced an estimated distance ($1550 \pm 166 \text{ pc}$) to V460 And. This value is well within the Gaia DR2 determination of distance ($1526_{-110}^{+128} \text{ pc}$) calculated from parallax using the Bailer-Jones bias correction (Bailer-Jones 2015). In the future, investigators using small- to modest-aperture instruments should be able to estimate M_V from parallax (π) data since Gaia DR2 covers a large percentage of stars brighter than $G\text{-mag} = 15$. In this case, since $d = 1526 \text{ pc}$, $A_V = 0.2489$, and $V_{\text{avg}} = 13.142$, the value estimated for M_V is 1.98 ± 0.17 , similar to that determined from Equation 3. Gaia DR2 also includes estimates for stellar parameters (Andrae *et al.* 2018) such as radius and luminosity. However, it is worth exploring differences between these values reported for V460 And in Gaia DR2 and those otherwise determined herein. First it should be noted that the Gaia passbands (BP, G, and RP) are unique (Jordi *et al.* 2010) so that transforms are needed should one desire conversion to other conventional photometric systems. For example, when color excess $(B-V)$ is known, Gaia G-magnitudes can be transformed to Johnson-Cousins V_{mag} according to the following expression (Equation 5):

$$G - V = a + b(B - V) + c(B - V)^2 + d(B - V)^3. \quad (5)$$

The appropriate Johnson-Cousins coefficients (a-d) can be found in Table 5.8 of Documentation Release 1.1 from Gaia Data Release 2 (<https://gea.esac.esa.int/archive/-documentation/GDR2/>). In this case using V460 And values

derived for G_{BP} (13.4026 ± 0.0174), G_{RP} (12.92 ± 0.011), and G (13.244 ± 0.0021), V_{mag} was calculated to be 13.296 ± 0.004 , a result close to the observed V_{min} (13.288 ± 0.010) for V460 And. Derivation of stellar parameters first released from the Gaia Mission is described in detail by Andrae *et al.* (2018). For the purposes of this paper the steps used to calculate luminosity and radius have been greatly simplified below. Absolute G-band magnitude (M_G) is estimated according to Equation 6:

$$M_G = G - 5 \cdot \log_{10}(r) + 5 - A_G, \quad (6)$$

where G is the photometric system magnitude, $r = 1/\pi$ (arcsec), and A_G is the interstellar extinction. In order to determine stellar luminosity, the calculated value for M_G is adjusted by the bolometric correction (BC_G) using the T_{eff} dependent polynomial coefficients provided in Table 4 and Equation 7 from Andrae *et al.* (2018). In this case $BC_G = 0.0608$, such that $M_{bol} = 2.278$ when $A_G = 0$. The assumed null value for A_G is an important distinction since non-Gaia data such as those determined from independently derived extinction maps are not used to produce absolute magnitude estimates. The luminosity of V460 And in solar units ($L_* = 9.65 \pm 1.6 L_\odot$) was calculated according to Equation 7:

$$L_* / L_\odot = 10^{(M_{bol\odot} - M_{bol*}) / 2.5}, \quad (7)$$

where $M_{bol\odot} = 4.74$ and $M_{bol*} = 2.278$. Finally, the radius of V460 And in solar units ($R_* = 1.84 \pm 0.20$) was estimated using the well-known relationship (Equation 8) where:

$$L_* / L_\odot = (R_* / R_\odot)^2 (T_* / T_\odot)^4. \quad (8)$$

It is very challenging to accurately determine the mass of a single isolated field star. Nonetheless, according to a model using MS stars in detached binary systems, Eker *et al.* (2018) developed a mass-luminosity relationship ($1.05 < M/M_\odot \leq 2.40$) according to Equation 9:

$$\log(L) = 4.329(\pm 0.087) \cdot \log(M) - 0.010(\pm 0.019). \quad (9)$$

This expression leads to a mass ($M_* = 1.71 \pm 0.07$) in solar units as derived from the Gaia DR2 stellar parameters where $L_* = 9.65 \pm 1.55 L_\odot$. All of these values (M_* , R_* , L_* , and T_{eff}) summarized in Table 4 fall well within expectations for a HADS variable. It bears repeating, however, that these fundamental physical parameters were derived by assuming that $A_G = 0$ according to Equation 6. As it turns out V460 And is in a region of the Milky Way (Gal. coord. (J2000): $l = 142.5144$; $b = -16.6884$) where interstellar extinction ($A_V = 0.2489$) should not be ignored. Therefore, the same equations (Equations 6–8) were applied but this time using the data obtained at DBO where $V_{avg} = 13.142 \pm 0.151$, $A_V = 0.2489 \pm 0.0019$, $M_V = 1.975$, and $BC_V = 0.0348$. The results summarized in Table 4 indicate that the Gaia DR2 reported values for luminosity and radius appear to be underestimated largely due to different assumptions about interstellar extinction. The greater luminosity ($12.36 \pm 2.69 L_\odot$) produced from the DBO data translates into a higher estimate for mass (1.82 ± 0.01) according to Equation 9. Furthermore,

stellar radius was independently estimated from an empirically-derived period-radius (P-R) relationship (Equation 10) reported by Laney *et al.* (2003) for HADS and classical Cepheids:

$$\log(R_*) = a + b \cdot \log(P) + c, \quad (10)$$

where $a = 1.106 \pm 0.012$, $b = 0.725 \pm 0.010$, and $c = 0.029 \pm 0.024$. In this case the value for R_* ($2.09 \pm 0.14 R_\odot$) was closer to the value obtained from observations at DBO ($2.15 \pm 0.38 R_\odot$). Other derived values for density (ρ_\odot), surface gravity ($\log g$), and pulsation constant (Q) are also included in Table 4. Stellar density (ρ_*) in solar units (g/cm^3) was calculated according to Equation 11:

$$\rho_* = 3 \cdot G \cdot M_* \cdot m_\odot / (4\pi (R_* \cdot r_\odot)^3), \quad (11)$$

where G = the gravitational constant ($6.67408 \cdot 10^{-8} \text{ cm}^3 \cdot \text{g}^{-1} \cdot \text{sec}^{-2}$), m_\odot = solar mass (g), r_\odot = solar radius (cm), M_* is the mass, and R_* the radius of V460 And in solar units. Using the same algebraic assignments, surface gravity ($\log g$) was determined by the following expression (Equation 12):

$$\log g = \log(M_* \cdot m_\odot / (R_* \cdot r_\odot)^2). \quad (12)$$

When attempting to characterize p-mode pulsations (radial) it is helpful to introduce the concept of a pulsation constant (Q). The dynamical time that it takes a p-mode acoustic wave to internally traverse a star is related to its size but more accurately the mean density. This is defined by the period-density relationship (Equation 13):

$$Q = P \sqrt{\bar{\rho}_* / \bar{\rho}_\odot} \quad (13)$$

where P is the pulsation period (d) and $\bar{\rho}_*$ and $\bar{\rho}_\odot$ are the mean densities of the target star and Sun, respectively. The mean density of an isolated field star like V460 And can not be determined without great difficulty. However, it can be expressed in terms (Equation 14) of other measurable stellar parameters where:

$$\log(Q) = -6.545 + \log(P) + 0.5 \log(g) + 0.1 M_{bol} + \log(T_{eff}). \quad (14)$$

The full derivation of this expression is provided in Breger (1990). The resulting Q values (Table 4) derived from observations at DBO are consistent with theory ($Q = 0.032$ d) and the distribution of Q -values (0.03 – 0.04 d) from fundamental radial pulsations observed with other δ Sct variables (Breger 1979; Joshi 2015; Antonello and Pastori 1981).

Finally, we attempted to get a relative sense of how the physical size, temperature, and brightness of V460 And changes over the course of a single 1.8-hr pulsation. As shown in Figure 6 there is a significant increase in reddening ($B-V$) as maximum light descends to minimum light. Intrinsic color reveals that at maximum light, where $(B-V)_0 = 0.181 \pm 0.006$, the corresponding effective temperature is 7883 ± 263 K, whereas at minimum light ($(B-V)_0 = 0.313 \pm 0.010$) the estimated effective temperature is 7151 ± 229 K. Between these two extremes the putative rise in temperature ($+732$ K) would correspond to a 1.5-

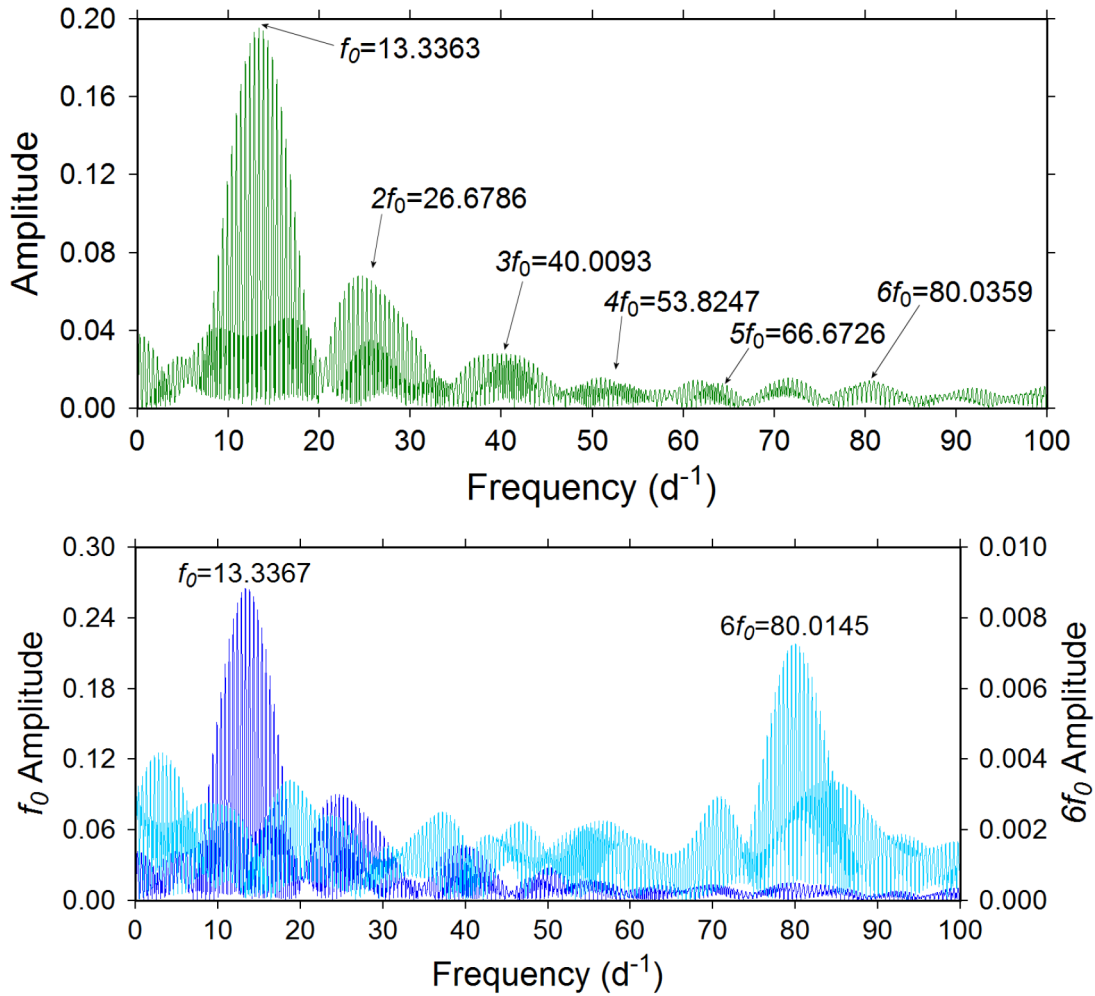


Figure 7. Unwhitened V-mag amplitude spectrum (top) showing all significant pulsation frequencies following DF_T analysis of photometric data from V460 And acquired in 2018 at DBO. The bottom amplitude spectra (B-mag) illustrate the fundamental (f_0) frequency and its highest partial harmonic ($6f_0$), which was clearly detected ($S/N \geq 4$) following prewhitening.

fold increase in luminosity but only a relatively small increase ($+0.02 R_\odot$) in radius. This rather crude estimate for changes in stellar radius would be best performed using the Baade-Wesselink method developed by Wesselink (1946) should radial velocity data over an entire oscillation cycle become available for this system.

3.5. Kinematics

Stellar kinematics on field stars have been used (Balona and Nemeč 2012, hereafter BN2012) to ostensibly discriminate between Pop. I HADS and its sibling Pop. II SX Phe-type variables found during the Kepler Mission (Gilliland *et al.* 2010). This potentially important observation arrives at a time when new results from space telescopes indicate that SX Phe variables are not necessarily high amplitude, low luminosity, or metal-poor (Nemeč *et al.* 2017). It would appear that the canonical definition of SX Phe variables likely suffers from observational bias due to the sensitivity limitations of ground-based telescopes. Gaia DR2 (Gaia *et al.* 2016, 2018) provides highly accurate data for proper motion (PM) and parallax from nearly 80 million sources ($G \leq 15$ mag) that fall within the light grasp of small (100 to 400 mm) aperture telescopes. PM (μ_α in

R.A. and μ_δ in Dec.) must be understood within the context of where the star resides; it may appear to be large when relatively close to the Sun or diminishingly small at much greater distances. Gaia DR2 (Sartoretti *et al.* 2018) only includes radial velocity (RV) data from stars with an effective temperature between 3500 and 7000 K, thereby eliminating the possibility of calculating space velocity for V460 And along with most other HADS variables. According to BN2012, another discriminating measure of motion relative to the Sun may be tangential velocity (V_T), which factors in distance according to the relationship (Equation 15):

$$V_T = 4.74 \cdot \mu \cdot d \quad (15)$$

where V_T is in km s^{-1} , $\text{PM} = \mu_\alpha$ or μ_δ (mas y^{-1}), and d is the distance in kpc. For V460 And, substituting the Gaia DR2 values for PM ($\mu_\alpha = -0.134 \pm 0.061$ and $\mu_\delta = -2.976 \pm 0.067$ mas y^{-1}) and distance ($d = 1.526$ kpc) lead to V_T values of -0.97 ± 0.45 ($V_{T\alpha}$) and $-21.53 - 1.87$ ($V_{T\delta}$). By comparison it would appear that the $V_T (> 120 \text{ km s}^{-1}$ in R.A. or Dec.) of SX Phe variable candidates in the Kepler field (BN2012) far exceed the corresponding velocities observed for V460 And (Table 5). On the strength of

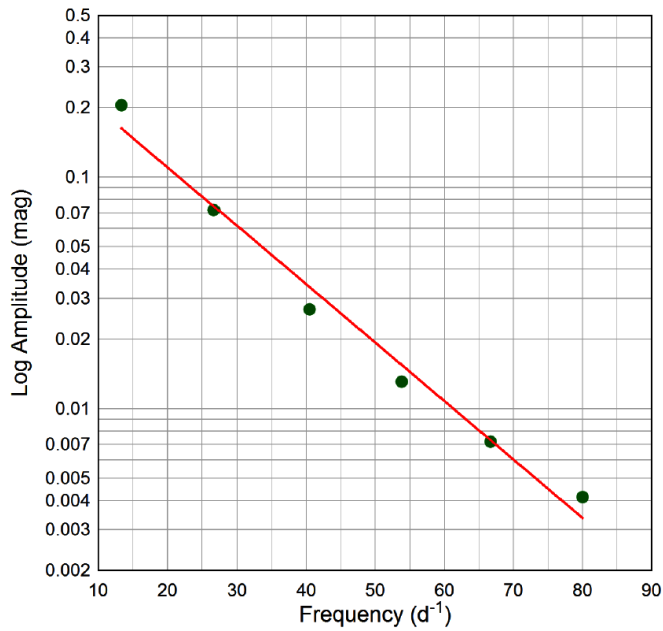


Figure 8. Amplitude decay of the fundamental (f_0) pulsation period and its corresponding partial harmonics ($2f_0-6f_0$) observed in the B-passband.

these results, can V460 And be unambiguously classified as a HADS and not an SX Phe variable? Unfortunately, the results generated in BN2012 proved to be much less compelling when comparisons were made using data from Gaia DR2 instead of the UCAC3 catalog (Zacharias *et al.* 2010). This can be seen in Table 5 which compares kinematics from candidate SX Phe stars (Table 1 in BN2012) to those recalculated using PM and distances (Bailer-Jones 2015) from Gaia DR2. This assessment also includes the same kinematics from a group of HADS variables located in Lyra and Cygnus which are classified as such in the International Variable Star Index (VSX). As illustrated in Figure 10, for the most part the HADS variables identified in VSX co-mingle with the central cluster of the SX Phe candidates and V460 And. Far fewer SX Phe candidates (3 vs. 34) emerge that appear to have V_T values significantly different (circle radius = 1σ) from the mean value. In addition those SX Phe candidates positioned within 1σ of the mean capture the full range of $[Fe/H]$ values provided in BN2012 with no bias towards solar-like metallicity. RR Lyrae variables were included by BN2012 as a positive control since they were known to be very metal-poor ($-2.54 > [Fe/H] > -0.42$) and estimated to reside at even greater distances (1.5–16.1 kpc). However when V_T was recalculated using Gaia DR2-derived values for PM (Table 6) and distance, less than half (10/22) fell outside the variability (1σ) observed with known HADS

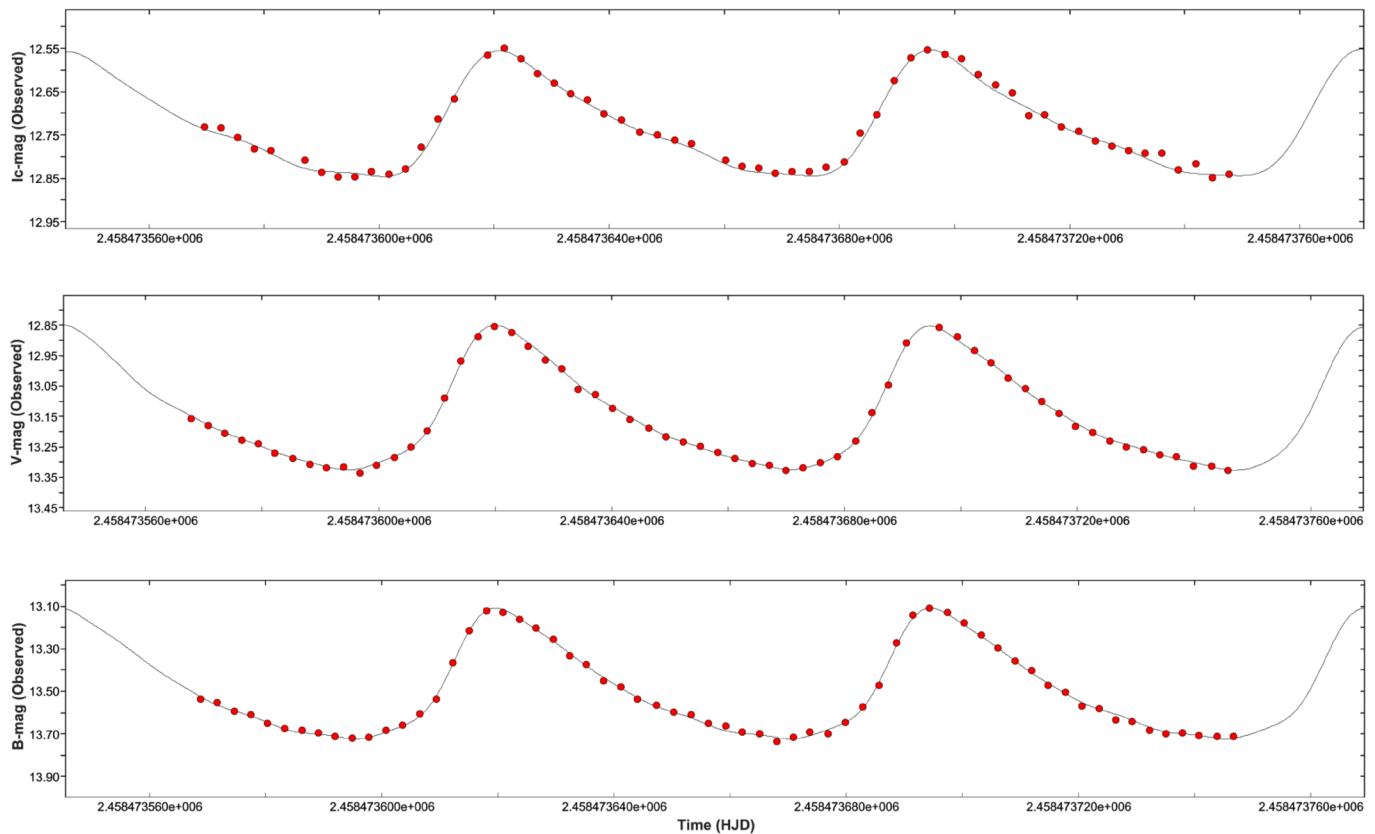
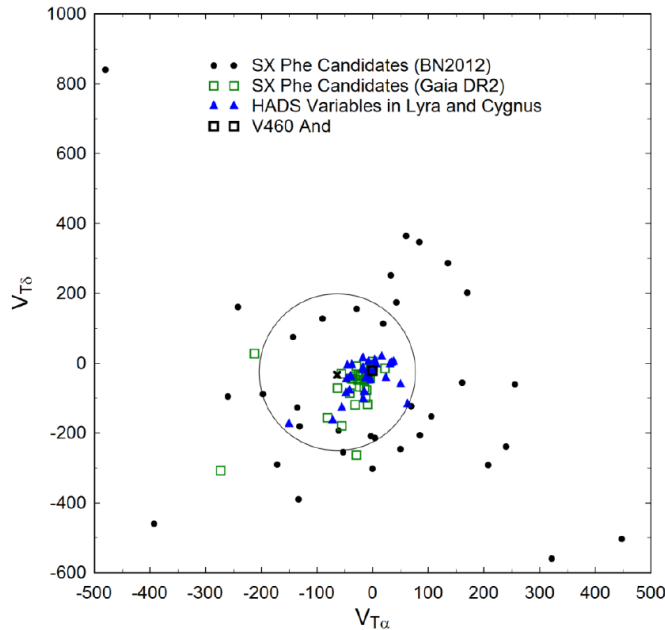


Figure 9. Representative fit of B- (bottom), V- (middle), and I_c -mag (top) time series data based on elements derived from DFT. These data were acquired on Dec. 21, 2018 at DBO.

Table 4. Global stellar parameters for V460 And using Gaia DR2 derived values and those determined directly from observations at DBO.

Parameter	Gaia DR2	DBO
Mean T_{eff} [K]	7507 ± 427	7385 ± 520
Mass [M_{\odot}]	1.71 ± 0.07	1.82 ± 0.01
Radius [R_{\odot}]	1.84 ± 0.20	2.15 ± 0.38
Luminosity [L_{\odot}]	9.65 ± 1.55	12.36 ± 2.69
ρ [g/cm^3]	0.386 ± 0.127	0.258 ± 0.139
$\log g$ [cgs]	4.14 ± 0.10	4.03 ± 0.14
Q [d]	0.0393 ± 0.005	0.0321 ± 0.006


 Figure 10. Comparison of tangential velocities ($V_{T\alpha}$ and $V_{T\beta}$) for putative SX Phe stars in the Kepler field using results from BN2012 (\bullet) and those calculated herein with proper motion and distances from Gaia DR2 (\square). Known HADS variables in Lyra and Cygnus (VSX) (\blacktriangle) show very little differentiation from all but three SX Phe candidates.

variables in the same region of the sky (Figure 11). In essence, V_T by itself does not offer a reliable means to determine whether V460 And can be unequivocally classified as a HADS variable. A noteworthy calculation (Equation 16):

$$z = d \cdot \sin(b), \quad (16)$$

where d is distance in pc (1526) and b is the Galactic latitude (-16.688°), places V460 And nearly 440 pc below the Galactic plane, territory also occupied by stars in the thick disk. Given these seemingly contradictory results, a more provocative question posits whether there is any unique set of features that allows one to classify a field star as a HADS or SX Phe-type pulsating variable.

3.6. Evolutionary status of V460 And

Knowing the luminosity and effective temperature of V460 And we can attempt to describe the evolutionary status of this variable. These values are plotted in the theoretical Hertzsprung-Russell diagram (HRD) shown in Figure 12. Here, the thick solid line gives the ZAMS position for stars with

solar metallicity while two broken lines nearly perpendicular to the ZAMS delimit the blue and red edges of the theoretical instability strip for radial low- p modes (Xiong *et al.* 2016). Asterisks mark the positions of several known HADS, both δ Scuti and SX Phe types (Balona 2018). The open circle indicates the position of V460 And using the DBO-derived parameters and corresponding error estimates provided in Table 4. To determine the mass and age of V460 And from theoretical evolutionary tracks its metallicity, Z , needs to be known. Unfortunately, this star has not been observed spectroscopically so no direct measurement of Z exists, however, we can at least try to estimate its value indirectly. V460 And has low tangential velocity (Figure 10), suggesting its affiliation with the galactic disc. Also its distance from the galactic plane favors a thick disc membership rather than halo. We can therefore assume that V460 And approaches solar metallicity, or at most a few times lower which also corresponds to the metallicity of metal-rich globular clusters classified as Oosterhoff type I.

But what is the true value of the solar metallicity? The numbers obtained in the last few decades range between 0.012 and 0.020, with the recently derived one of $Z_{\odot} = 0.0142$ (Asplund *et al.* 2009). However, very recently von Steiger and Zurbuchen (2016) questioned this result and obtained the value of $Z_{\odot} = 0.0196 \pm 0.0014$ based on the analysis of the chemical composition of the solar wind. Yet, Serenelli *et al.* (2016) quickly showed that the derived composition is in serious disagreement with the observables of the basic solar model so it cannot be representative of the solar interior. Obviously, the problem of a precise value for Z_{\odot} still remains open. We plot two series of PARSEC evolutionary models (Bressan *et al.* 2012) in Figure 12 wherein red solid lines show the models with $Z = 0.020$ and blue, dash-dotted lines define the models with $Z = 0.004$. The latter models would correspond to a decrease in metallicity by a factor of 3 to 5, depending on the reference solar metallicity. Assuming $Z = 0.020$, it can be seen (Figure 12) that V460 And has a solar mass of 1.75 ± 0.05 , solar radius of 2.15 ± 0.26 , and an age of 1.11 Gyr. Alternatively a metal poor ($Z = 0.004$) star would likely be smaller ($R_{\odot} = 2.0 \pm 0.26$), less massive ($M_{\odot} = 1.43 \pm 0.03$), and older (2.0 Gyr). Although V460 And lies closer to ZAMS than most of the plotted variables, it is an MS object which lies well within the instability strip among the other HADS. Uncertainty in the determination of mass will hopefully improve in the future should spectroscopic data become available for the V460 And.

4. Conclusions

This first multi-color (BVI_c) CCD study of V460 And has produced six new times-of-maximum which along with other published values lead to an updated linear ephemeris. Potential changes in the pulsation period assessed using the observed and predicted times-of-maximum suggests that since 1999 no significant change has occurred. Deconvolution of time-series photometric data by discrete Fourier transformation indicates that V460 And is a monophasic radial pulsator ($f_0 \approx 13.336 \text{ d}^{-1}$) which also oscillates in at least five other partial harmonics ($2f_0 - 6f_0$). Lacking a definitive classification spectrum, the intrinsic color, $(B - V)_0$, determined from this study was

Table 5. Proper motion (μ) and tangential velocity (V_T) for putative SX Phe stars in the Kepler field reported in BN2012 and those determined herein using data derived from Gaia DR2.

Kepler ID	BN2012					Gaia DR2				
	μ_α^a	μ_δ^a	d^b	$V_{T\alpha}^c$	$V_{T\delta}^c$	μ_α	μ_δ	d	$V_{T\alpha}$	$V_{T\delta}$
KIC 1162150	-33.1	37.6	0.7	-90	128	0.0	1.0	1.0	0	5
KIC 3456605	1.3	-48.4	0.9	4	-214	-1.9	-5.5	2.6	-23	-68
KIC 4168579	36.0	-39.2	1.6	208	-292	-2.2	-7.4	1.4	-15	-50
KIC 4243461	-74.4	-21.4	0.9	-260	-96	-2.5	-4.6	2.2	-26	-48
KIC 4662336	0.0	-62.1	1.0	0	-303	0.1	-1.9	1.5	1	-13
KIC 4756040	28.5	-31.6	1.0	106	-153	-0.8	-7.2	1.3	-5	-43
KIC 5036493	-1.1	-45.1	1.0	-3	-209	-5.6	-7.0	1.4	-36	-45
KIC 5390069	-11.9	47.6	0.7	-29	155	-0.9	-7.7	2.7	-12	-100
KIC 5705575	92.4	-78.5	1.3	448	-504	-1.5	-7.4	2.0	-15	-71
KIC 6130500	59.9	-11.0	1.2	256	-62	-4.8	-5.6	1.7	-38	-44
KIC 6227118	21.8	-28.4	4.2	322	-561	-2.3	-7.9	1.1	-12	-42
KIC 6445601	-55.6	-18.7	1.0	-197	-89	-1.0	-7.2	2.2	-11	-77
KIC 6520969	-42.5	21.0	1.6	-242	160	-40.2	5.1	1.1	-212	27
KIC 6780873	-24.5	-56.7	0.7	-61	-193	-1.0	-5.2	1.8	-8	-45
KIC 7020707	-32.6	-22.6	1.2	-135	-127	-0.2	-1.2	1.5	-2	-8
KIC 7174372	-35.7	-76.7	1.1	-133	-390	-5.1	-9.8	3.4	-81	-157
KIC 7300184	-45.7	-46.5	0.8	-131	-182	-2.1	-7.0	5.4	-55	-180
KIC 7301640	44.2	-11.2	1.0	161	-56	-0.4	-0.6	1.3	-3	-4
KIC 7621759	8.9	48.1	1.1	33	251	-0.5	-6.0	1.5	-4	-42
KIC 7765585	27.7	81.2	0.4	43	173	-3.0	-3.6	2.2	-32	-38
KIC 7819024	11.6	-41.1	1.3	50	-246	-1.0	-14.1	1.8	-9	-118
KIC 8004558	-11.1	-38.4	1.4	-53	-256	-4.5	-41.1	1.4	-29	-263
KIC 8110941	-46.8	17.5	0.9	-143	74	-1.6	-6.3	4.0	-31	-120
KIC 8196006	24.4	-31.2	0.8	69	-124	2.7	-1.9	1.7	22	-15
KIC 8330910	39.0	59.2	1.0	135	286	-1.2	-5.7	1.4	-8	-39
KIC 9244992	40.2	-28.2	1.8	240	-240	-7.0	-3.9	1.7	-56	-31
KIC 9267042	-79.0	96.5	1.8	-480	840	-2.8	-0.9	2.2	-29	-9
KIC 9535881	6.9	28.2	0.8	19	113	-3.7	-4.8	1.4	-25	-33
KIC 9966976	19.1	53.8	1.4	84	346	-1.3	-5.6	1.5	-9	-39
KIC 10989032	-68.0	-52.8	1.8	-393	-460	-1.9	-3.1	2.4	-21	-35
KIC 11649497	21.4	-33.6	1.3	85	-206	-4.6	-9.6	1.9	-41	-86
KIC 11754974	-53.2	-57.7	1.1	-172	-291	-51.7	-58.3	1.1	-273	-308
KIC 12643589	98.6	72.4	0.6	170	201	-0.4	-1.9	1.7	-3	-16
KIC 12688835	9.5	35.2	2.2	60	364	-4.0	-4.6	3.3	-63	-72

^a μ_α = proper motion (mas y^{-1}) in R.A. and μ_δ = proper motion (mas y^{-1}) in Dec.

^b d = distance in kpc.

^c $V_{T\alpha}$ = tangential velocity (km s^{-1}) in R.A. and $V_{T\delta}$ = tangential velocity (km s^{-1}) in Dec.

used to estimate a mean effective temperature for V460 And (7385 ± 520 K); this corresponds to spectral type A9-F1. These results along with the distance estimate (1550 ± 166 pc) agreed quite well with the same findings (1526^{+128}_{-110} pc) provided in Gaia DR2. The pulsation period (0.07498076 d), oscillation mode (radial), V_{mag} amplitude (0.47 mag), and light curve morphology are all consistent with the defining characteristics of a HADS variable. Even if a metallicity ([Fe/H]) determination was available, these criteria do not necessarily exclude the possibility that V460 And is an example of a field SX Phe-type pulsator. In this case, the estimated mass of V460 And ($1.70\text{--}1.80 M_\odot$) according to Eker *et al.* (2018) exceeds the generally accepted threshold ($M < 1.3 M_\odot$) for SX Phe stars (McNamara 2011). Furthermore, evolutionary tracks from the PARSEC model which assume near solar abundance ($Z=0.020$) for V460 And are best matched by a MS star with a mass of $1.75 \pm 0.05 M_\odot$ and radius of $2.15 R_\odot$. Given these results, the sum total of evidence points to a HADS rather than an SX Phe variable. Unlike previously published findings (BN2012), a kinematic assessment using data from Gaia DR2 failed to prove that

tangential velocity alone could be used to differentiate HADS from SX Phe stars. New results arriving from various space telescopes appear to contradict the traditional definition for each type, belying the notion that field stars like V460 And can be neatly classified as HADS or SX Phe variables.

5. Acknowledgements

This research has made use of the SIMBAD database operated at Centre de Données astronomiques de Strasbourg, France. Time-of-maximum light data from the *Information Bulletin on Variable Stars* website proved invaluable to the assessment of potential period changes experienced by this variable star. In addition, the Northern Sky Variability Survey hosted by the Los Alamos National Laboratory, the International Variable Star Index maintained by the AAVSO, and the Catalina Sky Survey (CSDR1) maintained at CalTech were mined for critical information. This work also presents results from the European Space Agency (ESA) space mission Gaia. Gaia data are being processed by the Gaia Data Processing

Table 6. Proper motion (μ) and tangential velocity (V_T) of RR Lyae stars in the Kepler field reported in BN2012 and those determined herein using data derived from Gaia DR2.

Kepler ID	BN2012					Gaia DR2				
	μ_α^a	μ_δ^a	d^b	$V_{T\alpha}^c$	$V_{T\delta}^c$	μ_α	μ_δ	d	$V_{T\alpha}$	$V_{T\delta}$
KIC3733346	-17.1	-3.5	2.7	-221	-45	-17.05	-6.38	2.890	-233.49	-87.42
KIC3864443	-13.3	9.8	10.4	-658	484	-3.23	3.77	5.792	-88.60	103.48
KIC4484128	-22.5	-27.9	9.4	-1000	-1241	-0.60	-1.3	8.357	-23.65	-51.58
KIC5299596	-7.1	9.1	9.5	-322	410	-3.33	-6.01	4.161	-65.66	-118.43
KIC5559631	5.9	10.6	6.7	187	338	5.94	2.00	4.617	130.01	43.85
KIC6070714	-7.8	-1	9.4	-346	-44	-2.18	-5.54	5.226	-54.10	-137.12
KIC6100702	3.9	10.3	3.9	73	190	-0.61	0.77	3.106	-9.01	11.26
KIC6183128	-14.3	18.6	14.2	-959	1251	-0.58	0.26	6.285	-17.22	7.69
KIC6763132	-0.9	-1.9	3.3	-14	-29	-0.09	-1.05	3.054	-1.25	-15.23
KIC6936115	3.4	10.2	3	48	144	7.49	9.67	3.026	107.43	138.70
KIC7505345	4.4	-1.1	5.2	109	-27	1.67	5.51	4.406	34.94	114.96
KIC7742534	-6.4	-6.1	12.6	-380	-364	-0.52	-1.29	5.960	-14.80	-36.50
KIC7988343	-9.6	6.2	6.3	-287	184	-10.22	4.61	4.781	-231.56	104.38
KIC8344381	-2.3	2.2	15.3	-170	159	-1.54	-0.44	4.261	-31.08	-8.97
KIC9578833	0.3	16.5	16.1	21	1261	0.89	-1.13	7.379	31.23	-39.38
KIC9591503	-3.6	9	3.6	-62	154	-5.06	11.90	3.707	-88.98	209.04
KIC9697825	-3.9	10.1	14.2	-261	681	-2.30	0.36	8.210	-89.66	13.82
KIC9947026	1.4	8	3.6	23	137	-5.63	-6.63	3.475	-92.70	-109.23
KIC10136240	6.3	19.3	10.7	317	979	-0.67	0.25	5.194	-16.59	6.11
KIC10789273	5.5	-1.1	4.5	117	-23	5.83	9.05	8.378	231.39	359.22
KIC11125706	-6	-12.8	1.5	-42	-90	-8.07	-14.61	1.546	-59.13	-107.05
KIC11802860	-7.9	-3.9	3.2	-120	-59	-9.89	-6.23	3.031	-142.05	-89.57
KIC12155928	12.9	14.1	8.1	492	539	0.73	0.15	6.516	22.42	4.73

^a μ_α = proper motion (mas y^{-1}) in R.A. and μ_δ = proper motion (mas y^{-1}) in Dec.

^b d = distance in kpc.

^c $V_{T\alpha}$ = tangential velocity (km s^{-1}) in R.A. and $V_{T\delta}$ = tangential velocity (km s^{-1}) in Dec.

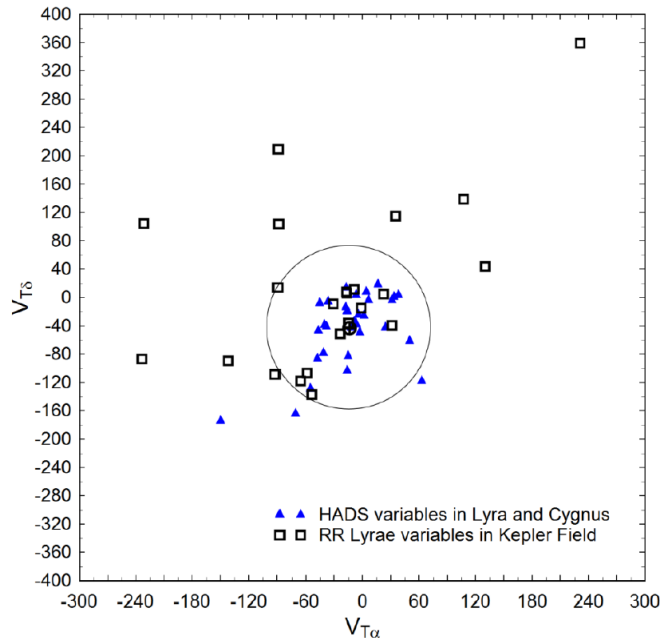


Figure 11. Comparison of tangential velocities ($V_{T\alpha}$ and $V_{T\delta}$) for RR Lyrae stars in Kepler field (\square) and known HADS variables in Lyra and Cygnus (\blacktriangle) using proper motion and distances from Gaia DR2. The significant overlap challenges the notion that V_T alone can be used to classify pulsating variables.

and Analysis Consortium (DPAC). Funding for the DPAC is provided by national institutions, in particular the institutions participating in the Gaia MultiLateral Agreement (MLA). The Gaia mission website is <https://www.cosmos.esa.int/gaia>. The Gaia archive website is <https://archives.esac.esa.int/gaia>. This paper makes use of data from the first public release of the WASP data (Butters *et al.* 2010) as provided by the WASP consortium and services at the NASA Exoplanet Archive, which is operated by the California Institute of Technology, under contract with the National Aeronautics and Space Administration under the Exoplanet Exploration Program. The diligence and dedication shown by all associated with these organizations is very much appreciated. We gratefully acknowledge the careful review and helpful commentary provided by an anonymous referee.

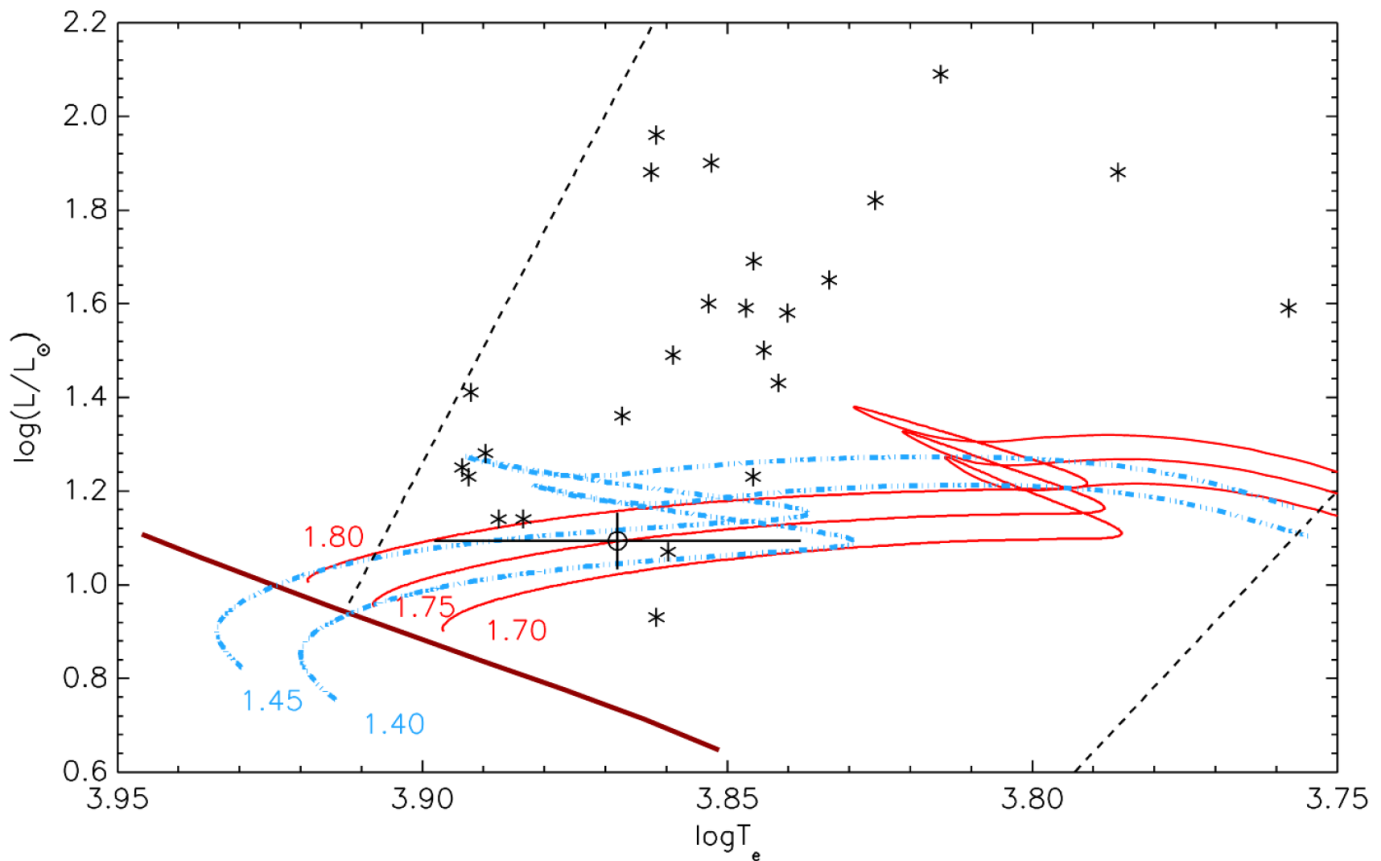


Figure 12. Evolutionary tracks (red solid line: $Z=0.020$ and blue dashed line: $Z=0.004$) derived from PARSEC models (Bressan *et al.* 2012) showing position of V460 And (circle) relative to ZAMS (thick maroon line) within the theoretical instability strip (dashed lines) for radial low- p mode pulsators. Asterisks denote the positions of known HADs (Balona 2018).

References

- Akerlof, C., *et al.* 2000, *Astron. J.*, **119**, 1901.
- Amôres, E. B., and Lépine, J. R. D. 2005, *Astron. J.*, **130**, 650.
- Amôres, E. B., and Lépine, J. R. D. 2007, *Astron. J.*, **133**, 1519.
- Andrae, R., *et al.* 2018, *Astron. Astrophys.*, **616A**, 8.
- Antonello, E., and Pastori, L. 1981, *Publ. Astron. Soc. Pacific*, **93**, 237.
- Asplund, M., Grevesse, N., Sauval, A. J., and Scott, P. 2009, *Ann. Rev. Astron. Astrophys.*, **47**, 481.
- Baade, W. 1956, *Publ. Astron. Soc. Pacific*, **68**, 5.
- Baglin, A. 2003, *Adv. Space Res.*, **31**, 345.
- Bailer-Jones, C. A. L. 2015, *Publ. Astron. Soc. Pacific*, **127**, 994.
- Baker, N., and Kippenhahn, R. 1962, *Z. Astrophys.*, **54**, 114.
- Baker, N., and Kippenhahn, R. 1965, *Astrophys. J.*, **142**, 868.
- Balona, L. A. 2018, *Mon. Not. Roy. Astron. Soc.*, **479**, 183.
- Balona, L. A. and Nemeč, J. M. 2012, *Mon. Not. Roy. Astron. Soc.*, **426**, 2413.
- Berry, R., and Burnell, J. 2005, *The Handbook of Astronomical Image Processing*, 2nd ed., Willmann-Bell, Richmond, VA.
- Breger, M. 1979, *Publ. Astron. Soc. Pacific*, **91**, 5.
- Breger, M. 1990, *delta Scuti Star Newsl.*, **2**, 13.
- Breger, M. 2000, *Baltic Astron.*, **9**, 149.
- Bressan, A., Marigo, P., Girardi, L., Salasnich, B., Dal Cero, C., Rubele, S., and Nanni, A. 2012, *Mon. Not. Roy. Astron. Soc.*, **427**, 127.
- Burstein, D., and Heiles, C. 1978, *Astrophys. J.*, **225**, 40.
- Burstein, D., and Heiles, C. 1982, *Astron. J.*, **87**, 1165.
- Butters, O. W., *et al.* 2010, *Astron. Astrophys.*, **520**, L10.
- Casagrande, L., Ramírez, I., Meléndez, J., Bessell, M., and Asplund, M. 2010, *Astron. Astrophys.*, **512A**, 54.
- Chevalier, C. 1971, *Astron. Astrophys.*, **14**, 24.
- Cox, J. P. 1963, *Astrophys. J.*, **138**, 487.
- Drake, A. J., *et al.* 2009, *Astrophys. J.*, **696**, 870.
- Drimmel, R., Cabrera-Lavers, A., and López-Corredoira, M. 2003, *Astron. Astrophys.*, **409**, 205.
- Dworak, T. Z., and Zieba, S. 1975, *Inf. Bull. Var. Stars*, No. 1005, 1.
- Eker, Z., *et al.* 2018, *Mon. Not. Roy. Astron. Soc.*, **479**, 5491.
- Elst, E. W. 1978, *Inf. Bull. Var. Stars*, No. 1442, 1.
- Flower, P. J. 1996, *Astrophys. J.*, **469**, 355.
- Frolov, M. S. 1969, *Astron. Tsirk.*, **505**, 1.
- Gaia Collaboration, *et al.* 2016, *Astron. Astrophys.*, **595A**, 1.
- Gaia Collaboration, *et al.* 2018, *Astron. Astrophys.*, **616A**, 1.
- Gilliland, R. L., *et al.* 2010, *Publ. Astron. Soc. Pacific*, **122**, 131.
- Henden, A. A., Levine, S. E., Terrell, D., Smith, T. C., and Welch, D. L. 2011, *Bull. Amer. Astron. Soc.*, **43**, 2011.

- Henden, A. A., Terrell, D., Welch, D., and Smith, T. C. 2010, *Bull. Amer. Astron. Soc.*, **42**, 515.
- Henden, A. A., Welch, D. L., Terrell, D., and Levine, S. E. 2009, *Bull. Amer. Astron. Soc.*, **41**, 669.
- Hübsher, J. 2014, *Inf. Bull. Var. Stars*, No. 6118, 1.
- Hübsher, J., and Lehmann, P. B. 2012, *Inf. Bull. Var. Stars*, No. 6026, 1.
- Holdsworth D. L., et al. 2014, *Mon. Not. Roy. Astron. Soc.*, **439**, 2078.
- Jordi, C., et al. 2010, *Astron. Astrophys.*, **523A**, 48.
- Joshi, S., and Joshi, Y. C. 2015, *J. Astrophys. Astron.*, **36**, 33.
- Jurcsik, J., et al. 2005, *Astron. Astrophys.*, **430**, 1049.
- Khruslov, A. V. 2005, *Perem. Zvezdy Prilozh.*, **5**, 5.
- Kinman, T. D., Mahaffey, C. T., and Wirtanen, C. A. 1982, *Astron. J.*, **87**, 314.
- Kukarkin, B. V., Parenago, P. P., Efremov, Yu. N., and Kholopov, P. N. 1951, *Catalogue of Suspected Variable Stars*, Academy of Sciences USSR Sternberg, Moscow.
- Laney, C. D., Joneer, M., and Rodriguez, E. 2003, in *Interplay of Periodic, Cyclic and Stochastic Variability in Selected Areas of the H-R Diagram*, ed. C. Sterken, ASP Conf. Ser. 292, Astronomical Society of the Pacific, San Francisco, 203.
- Leavitt, H. S., and Pickering, E. C. 1912, *Circ. Harvard Coll Obs.*, No. 173, 1.
- Lee, Y.-H., Kim, S. S., Shin, J., Lee, J., and Jin, H. 2008, *Publ. Astron. Soc. Japan*, **60**, 551.
- Lenz, P., and Breger, M. 2005, *Commun. Asteroseismology*, **146**, 53.
- Lindgren, L., et al. 2016, *Astron. Astrophys.*, **595A**, 4.
- Longmore, A. J., Fernly, J. A., and Jameson, R. F. 1986, *Mon. Not. Roy. Astron. Soc.*, **220**, 279.
- McNamara, D. H. 2000, in *Delta Scuti and Related Stars*, ASP Conf. Ser., 210, ed. M. Breger, M. Montgomery, Astronomical Society of the Pacific, San Francisco, 373.
- McNamara, D. H. 2011, *Astron. J.*, **142**, 110.
- Minor Planet Observer. 2011, MPO Software (<http://www.minorplanetobserver.com>), BDW Publishing, Colorado Springs.
- Neeley, J. R., et al. 2015, *Astrophys. J.*, **808**, 11.
- Nemec, J. M., Balona, L. A., Murphy, S. J., Kinemuchi, K., and Jeon, Y.-B. 2017, *Mon. Not. Roy. Astron. Soc.*, **466**, 1290.
- Niu, J.-S., Fu, J.-N., and Zong, W.-K. 2013, *Res. Astron. Astrophys.*, **13**, 1181.
- Niu, J.-S., et al. 2017, *Mon. Not. Roy. Astron. Soc.*, **467**, 3122.
- Paunzen, E., and Vanmunster, T. 2016, *Astron. Nachr.*, **337**, 239.
- Poretti, E. 2003a, *Astron. Astrophys.*, **409**, 1031.
- Poretti, E. 2003b, in *Interplay of Periodic, Cyclic and Stochastic Variability in Selected Areas of the H-R Diagram*, ed. C. Sterken, ASP Conf. Ser. 292, Astronomical Society of the Pacific, San Francisco, 145.
- Rodríguez E., and Breger, M. 2001, *Astron. Astrophys.*, **366**, 178.
- Sartoretti, P., et al. 2018, *Astron. Astrophys.*, **616A**, 6.
- Schlafly, E. F., and Finkbeiner, D. P. 2011, *Astrophys. J.*, **737**, 103.
- Schlegel, D. J., Finkbeiner, D. P., and Davis, M. 1998, *Astrophys. J.*, **500**, 525.
- Schwarzenberg-Czerny, A. 1996, *Astrophys. J., Lett.*, **460**, L107.
- Serenelli, A., Scott, P., Villante, F. L., Vincent, A. C., Asplund, M., Basu, S., Grevesse, N., and Peña-Garay, C. 2016, *Mon. Not. Roy. Astron. Soc.*, **463**, 2.
- Skrutskie, M. F., et al. 2006, *Astron. J.*, **131**, 1163.
- Smith, T. C., Henden, A. A., and Starkey, D. R. 2011, in *The Society for Astronomical Sciences 30th Annual Symposium on Telescope Science*, The Society for Astronomical Sciences, Rancho Cucamonga, CA, 121.
- Software Bisque. 2013, THE SKYX Professional Edition 10.5.0 (<http://www.bisque.com>).
- Templeton, M. R., Samolyk, G., Dvorak, S., Poklar, R., Butterworth, N., and Gerner, H. 2009, *Pub. Astron. Soc. Pacific*, **121**, 1076.
- Torres, G. 2010, *Astron. J.*, **140**, 1158.
- Uytterhoeven, K., et al. 2011, *Astron. Astrophys.*, **534A**, 125.
- von Steiger, R., and Zurbuchen, T. H. 2016, *Astrophys. J.*, **816**, 13.
- Walker, G., et al. 2003, *Publ. Astron. Soc. Pacific*, **115**, 1023.
- Wesselink, A. J. 1946, *Bull. Astron. Inst. Netherlands*, **10**, 91.
- Wils, P., et al. 2009, *Inf. Bull. Var. Stars*, No. 5878, 1.
- Wils, P., et al. 2010, *Inf. Bull. Var. Stars*, No. 5928, 1.
- Wils, P., et al. 2011, *Inf. Bull. Var. Stars*, No. 5977, 1.
- Wils, P., et al. 2012, *Inf. Bull. Var. Stars*, No. 6015, 1.
- Wils, P., et al. 2013, *Inf. Bull. Var. Stars*, No. 6049, 1.
- Wils, P., et al. 2014, *Inf. Bull. Var. Stars*, No. 6122, 1.
- Wils, P., et al. 2015, *Inf. Bull. Var. Stars*, No. 6150, 1.
- Xiong, D. R., Deng, L., Zhang, C., and Wang, K. 2016, *Mon. Not. Roy. Astron. Soc.*, **457**, 3163.
- Zacharias, N., et al. 2010, *Astron. J.*, **139**, 2184.
- Zhevakin, S. A. 1963, *Ann. Rev. Astron. Astrophys.*, **1**, 367.
- Ziaali, E., et al. 2018, Physics of Oscillating Stars, Banyuls-sur-mer, France, DOI 10.5281/zenodo.1494351.